HHS Public Access

Author manuscript

J Bone Miner Res. Author manuscript; available in PMC 2024 January 31.

Published in final edited form as:

J Bone Miner Res. 2023 May ; 38(5): 765–774. doi:10.1002/jbmr.4798.

Sostdc1 suppression in the absence of sclerostin potentiates anabolic action of cortical bone in mice

Roy B. Choi[1], **April M. Hoggatt**[1], **Daniel J. Horan**[1], **Emily Z. Rogers**[1], **Gabriela G. Loots**[2], **Alexander G. Robling**[1,3,4,5]

[1.]Department of Anatomy, Cell Biology & Physiology, Indiana University School of Medicine, Indianapolis, IN, USA.

[2.]Department of Orthopaedic Surgery, School of Medicine, UC Davis Health, Sacramento, CA, USA.

[3.]Richard L. Roudebush Veterans Affairs Medical Center, Indianapolis, IN, USA

[4.]Department of Biomedical Engineering, Indiana University–Purdue University at Indianapolis, Indianapolis, IN, USA.

[5.]Indiana Center for Musculoskeletal Health, Indianapolis, IN, USA.

Abstract

The development of Wnt-based osteoanabolic agents have progressed rapidly in recent years, given the potent effects of Wnt modulation on bone homeostasis. Simultaneous pharmacologic inhibition of the Wnt antagonists sclerostin and Dkk1 can be optimized to create potentiated effects in the cancellous bone compartment. We looked for other candidates that might be co-inhibited along with sclerostin to potentiate the effects in the cortical compartment. Sostdc1 (Wise), like sclerostin and Dkk1, also binds and inhibits Lrp5/6 co-receptors to impair canonical Wnt signaling, but Sostdc1 has greater effects in the cortical bone. To test this concept, we deleted Sostdc1 and Sost from mice and measured the skeletal effects in cortical and cancellous compartments individually. Sost deletion alone produced high bone mass in all compartments, whereas Sostdc1 deletion alone had no measurable effects on either envelope. Mice with co-deletion of Sostdc1 and Sost had high bone mass and increased cortical properties (bone mass, formation rates, mechanical properties), but only among males. Combined administration of sclerostin antibody and Sostdc1 antibody in WT female mice produced potentiation of cortical bone gain despite no effect of Sostdc1 antibody alone. Sostdc1 inhibition/deletion can work in concert with sclerostin deficiency to improve cortical bone properties.

Keywords

Wnt; sclerostin; Sost; Sostdc1; Wise; ectodin; bone anabolism; osteoporosis

Corresponding author: Alexander G. Robling, Ph.D. Department of Anatomy, Cell Biology & Physiology, Indiana University School of Medicine, 635 Barnhill Dr., MS 5035, Indianapolis, IN 46202, Tel: (317) 274-7489, Fax: (317) 278-2040, arobling@iupui.edu.

Author Contributions

RBC and AGR designed the experiments and wrote the paper. RBC EZR, DJH collected and analyzed data. RBC, GGL and AMH contributed to mouse generation and assay design. RBC and AGR contributed to experimental design and data interpretation.

All authors have declared that no conflicts of interest exist.

INTRODUCTION

Skeletal fragility is a major health concern in the US, and its prevalence is tightly coupled to aging. The proportion of the population that is 65 and older is on the rise, and is expected to continue rising in the coming decades.[1] Therefore, the development of new approaches for treating skeletal fragility will be a key goal for improving health and reducing health care costs. There is growing appreciation for the significance of cortical bone *per se* in skeletal integrity and disease, though this compartment has received far less attention than cancellous bone, both experimentally and clinically.[2] Maintaining cortical bone health has some unique challenges compared to the cancellous compartment, including the effects of porosity/macroporosity, a high mean tissue age, and reduced proximity of resident osteocytes to the vasculature.

As we uncover more about the biological underpinnings for differences in cortical and cancellous bone homeostasis, it is reasonable to expect that ensuing development of compartment-selective therapeutics will be possible. One of the “natural clues” that might provide a starting point to compartment-selective targeting is the phenotypes created by mutations in certain genes that affect skeletal dynamic differently across bone envelopes. For example, loss-of-function mutations in *Notum* and *Wnt16* affect cortical bone (positively for Notum loss, and negatively for Wnt16 loss) but have no measurable effect on cancellous bone.[3, 4] Conversely, selective overexpression of Wnt10b in osteoblasts (Bglap-Cre) results in a strong cancellous bone phenotype but no effect on the cortical compartment.[5] Further, other genes can have diametrically opposed effects on cancellous vs. cortical compartments (e.g., sFrp4).[6]

Sostdc1 (Sclerostin domain containing-1; also known as Wise, Ectodin, or USAG1) is another gene whose protein product appears to elicit compartment-specific effects on the skeleton. Sostdc1 is the most closely-related cysteine knot paralog to the more highly studied sclerostin protein. Like sclerostin, Sostdc1 binds to the Wnt co-receptors/facilitators Lrp4/5/6 to disrupt canonical Wnt signaling—a key pathway in the development and maintenance of skeletal and dental tissues.[7-11] Sostdc1 is highly expressed in the periosteum, where it is known to modulate Wnt signaling during local fracture repair.[12] Mice with homozygous loss-of-function mutations in Sostcd1 ($Sostdc1^{-/-}$) have accelerated fracture healing, driven by enhanced periosteal bone formation.[12] $Sostdc1^{-/-}$ mice exhibit mildly increased cortical bone mass and formation rates compared to wild-type (WT) littermates, but cancellous properties are unchanged or slightly reduced compared to wild-type mice. In previous communications, we reported that the skeletal efficacy of Wnt inhibitor disruption (e.g., sclerostin neutralization) can be synergistically improved by simultaneous co-inhibition of other Wnt inhibitors, even if neutralization of those auxiliary inhibitors has no efficacy on their own.[13] This phenomenon was first demonstrated for Dkk1, where we and others[14] found that Dkk1 deletion or pharmacologic suppression had little to no effect on bone gain, but Dkk1 deletion or suppression on a $Sost^{-/-}$ background (or combined with sclerostin antibody) was potently osteoanabolic, well beyond the sclerostin neutralization effects. Curiously, we found consistent synergistic action of co-deletion/co-suppression for Dkk1 and Sost only in the cancellous compartment, but the

cortical compartment was additive.[13, 15, 16] This prompted us to begin looking for other synergistic partnerships for sclerostin neutralization that would preferentially target the cortical bone. The cortical phenotype observed in Sostdc1$^{-/-}$ mice[12] suggested a possible target to exploit, alongside sclerostin, to improve cortical bone selectively.

In this communication, we tested changes to the cortical compartment induced by co-deletion of Sostdc1 and Sost in the same mice, compared to each mutant singly (Sostdc1$^{-/-}$ and Sost$^{-/-}$) and wild-type (WT). As a control for compartment specificity, we also evaluated changes to the cancellous compartment. Further, we tested the interaction in an *in vivo* pharmacologic model, using a combination of sclerostin antibody (Scl-Ab) and Sostdc1 antibody (Sdc-Ab), compared to each reagent individually. Using both genetic and pharmacologic models, we found significant enhancement of many cortical properties when both Sost and Sostdc1 were disabled, despite very mild effects of Sostdc1 deletion/inhibition alone.

MATERIALS AND METHODS

Mice

To take a genetic approach to Sost and Sostdc1 co-deletion, we generated Sost;Sostdc1 double knockout (DKO) mice by breeding Sostdc1$^{-/-}$ mice with Sost$^{-/-}$ mice for several generations to generate wildtype, Sost$^{-/-}$ Sostdc1$^{-/-}$, and Sost;Sostdc1 DKO mice on a uniform C57BL6J background. The derivation of both Sost$^{-/-}$ and Sostdc1$^{-/-}$ mice have been reported elsewhere. Briefly, Sost$^{-/-}$ mice were generated by replacing the entire ORF with a lacZ cassette,[17] and the Sostdc1$^{-/-}$ mice were generated by disrupting most of exon 1 with a nlacZ/PGK-NeoR cassette on the antisense strand.[18] Genotyping was conducted using PCR on tail snips to distinguish WT from null alleles for each gene (Fig S1). For the antibody studies, 8-week old C57BL/6J female mice were purchased from the Jackson Laboratory and acclimatized for 1 week prior to experimentation. Mice were housed 3 to 5 per cage in 12-hour light/dark conditions and were fed Teklad (Madison, WI, USA) Global Diet (2018SX) ad libitum. Mice in the genetic study were allocated to each experimental group based on their genotype, without regard for any inclusion criteria (the first ~10 mice generated for each genotype were used). Mice in the antibody studies were randomly assigned to treatment group without regard for any inclusion criteria.

Study approval

All animal procedures were performed in accordance with relevant federal guidelines and conformed to the Guide for the Care and use of Laboratory Animals (8th Edition).[19] The animal facility at Indiana University is an AAALAC-accredited facility and all mouse procedures were performed in accordance with the IACUC guidelines and approvals.

Antibody injection

Details of the development of sclerostin neutralizing antibody have been reported elsewhere. Briefly, the sclerostin monoclonal antibody (Scl-mAb), which neutralizes mouse sclerostin, is a version of a mouse monoclonal antibody in which the amino acid sequence has been modified for use in rats.[20] Sostdc1 monoclonal antibody (Sdc-mAb) was generated by

immunizing Sostdc1$^{-/-}$ mice, and an antibody that recognized loop-2 was selected, tested, and validated for specificity and efficacy.[21] Antibodies were injected into mice beginning at 9 wks of age, subcutaneously, at 25 mg/kg twice per week. Vehicle treatment was the phosphate buffered saline, in which the antibodies were diluted. All mice were treated for a duration of 6 wks.

Dual-energy x-ray absorptiometry (DXA)

Collection of repeated DXA measurements on live mice have been described and validated elsewhere.[13] Briefly, isoflurane anesthetized mice in the genetic study were scanned on a PIXImus II (GE Lunar) densitometer at 4.5, 6, 9, 12, 16 and 20 weeks of age. The densitometer was calibrated at the beginning of each scan day using a plastic mouse density phantom provided by the manufacturer (BMD=0.0611 g/cm^3 ; fat= −1.2%). For the Scl/Sdc antibody studies, mice were scanned at the beginning of treatment (9 wks of age) and again at the terminal timepoint (16 wks of age). Bone mineral density (BMD) was measured for the whole body, lumbar spine (L3–L5), and right hindlimb using the Lunar ROI (Region of Interest) tools. DXA-derived BMD/BMC measurements, and those collected from other assays (see below) were taken in a blinded fashion so that the investigator was unaware of group assignment.

Microcomputed tomography (μCT)

Formalin-fixed femora and 5th lumbar vertebrae (L5) were scanned, reconstructed, and analyzed on a Scanco μCT-35 as previously described.[15, 22] 10-μm resolution, 50-kV peak tube potential and 151-ms integration time were used. Standard parameters related to cancellous and cortical bone architecture were measured.

Fluorochrome administration and bone quantitative histomorphometry

For the genetic studies, each mouse was injected with 200μL of calcein (12 mg/kg, i.p.) at 4.5 wks of age, oxytetracycline HCl (80 mg/kg) at 9 wks of age, demeclocycline (40 mg/kg, i.p.) at 16 wks of age, and alizarin complexone (20 mg/kg, i.p.) at 19 and 19.5 wks of age to label mineralizing bone throughout the experimental period. After sacrifice (at 20 wks of age), one of the femurs from each mouse was processed for plastic-embedded histomorphometry and cut at midshaft for histological evaluation as previously described.[15, 23] Briefly, periosteal and endocortical mineralizing surface (MS/BS, %), mineral apposition rates (MAR; μm/day) and bone formation rates (BFR/BS; μm^3/μm^2/yr) were calculated using the oxytetracycline and the middle of double alizarin complexone labels, measured over the entire periosteal and endocortical surfaces (not subregions) according to standard protocols.

For the analysis of osteoclast parameters, after conducting μCT measurements on the distal femur, we processed those tissues for plastic-embedded thin sectioning and Trap-staining as described previously. Briefly, distal femur samples were re-embedded in methylmethacrylate, sectioned at 6 μm using a motorized microtome equipped with a tungsten-carbide knife, and the sections were flattened onto charged slides. Each slide was stained for Trap and countered with Toluidine blue to visualize osteoclasts, as previously described.[24] Sections were read for osteoclast number and perimeter using

the OsteoMeasure system (OsteoMetrics Inc., Decatur, GA, USA), according to standard protocols.

For the antibody studies, mice were given 200μL injections of demeclocycline (40 mg/kg, i.p.) at the beginning of treatment (9 wks of age), calcein (12 mg/kg, i.p.) at 5th week of treatment, and alizarin complexone (20 mg/kg, i.p.) at 6th week of treatment to label mineralizing bone throughout the experimental period. Mice were sacrificed 3 days after the alizarin label. After sacrifice, the femurs were processed for histological sectioning and measurements as described above. Alizarin labels were injected into mice (and thus they appear in the histology images shown) but were not used for measurements.

Whole bone mechanical properties

Parameters related to whole bone strength were measured using 3-point bending tests as previously described.[15] Briefly, each femur was thawed to room temperature and loaded to failure in monotonic compression using 3-point bending platens. The lower span points were spaced 10 mm, and the upper point contacted the femoral diaphysis at midshaft. During each test, force and displacement were collected every 0.01 seconds. From the force/displacement curves, ultimate force and energy to failure were calculated using standard equations.[25]

Statistical analysis

Statistical analyses were performed using the JMP package (version 4.0, SAS Institute Inc.). Radiographic, histomorphometric, biomechanical endpoints were analyzed using two-way ANOVA followed by Tukey post hoc test. Time series data like DXA and body mass were analyzed with repeated-measures ANOVA followed by Tukey post hoc test. When at least one main effect was significant, interactions terms were calculated and tested for significance. Statistical significance is indicated in figures by displaying actual p-values. DXA data were presented as mean ± SD. Remaining date sets are presented in box-and-whisker format with scatter variates superimposed.

RESULTS

Co-deletion of Sost and Sostdc1 in male mice improves bone mineral density and content beyond Sost deletion alone.

To investigate the potential of Sost and Sostdc1 co-deletion to improve bone gain in mice, we generated Sost;Sostdc1 double knockout (DKO) mice and all controls (Sost KO alone, Sostdc1 KO alone, WT) and measured the skeletal phenotype during growth and maturation using serial DXA (Fig. 1A). Body mass, measured intermittently from 4.5 to 20 weeks of age, was not significantly different among the 4 genotypes, for both males and females (Fig. 1B). Bone mineral density (BMD) and bone mineral content (BMC) were measured from whole body scans collected intermittently over the same time 4.5-20 wk span, and three regions of interest (ROIs) were analyzed from each scan: whole body, lumbar spine, and hindlimb. As expected, Sost-KO exhibited a significant increase in BMD over WT controls, at all three ROIs in both males and females (Fig. 1C). Conversely, BMD in Sostdc1-KO mice was not significantly different from WT controls, for either sex and at any ROI (Fig. 1C). Male mice with compound deletion of Sost and Sostdc1 exhibited significant

improvement in BMD compared to the already high bone mass Sost-KO, at all three ROIs. Female DKOs exhibited more muted effects of the compound mutations compared to Sost-KO, with two of the three ROIs reaching near significant ($p = 0.06$-0.09) differences (Fig. 1C). Similar outcomes were observed for BMC (Fig. S1). Taken together, the results suggest that Sostdc1 deletion significantly increases DXA-derived bone mass only on a Sost-deficient background (but not on a $Sost^{+/+}$ background), mainly in male mice.

Co-deletion of Sost and Sostdc1 improves cortical bone properties in male mice and cancellous bone properties in female mice, compared to Sost deletion alone.

To parse out the DXA-based results by bone compartment and achieve a better understanding the anabolic effects of Sost;Sostdc1 co-deletion on skeletal properties, we assessed μCT-derived parameters of femur and lumbar vertebrae from mice in each of the 4 different genotypes. As expected, Sost deletion alone had significant positive effects on both cancellous and cortical bone, in both sexes (Fig. 2). Similar to the results reported for DXA-based measurements, Sostdc1 mice were not significantly different from WT controls for any of the μCT-based cortical or cancellous measurements. μCT–derived cortical bone properties at the midshaft femur, including cortical and total bone area (Ct.B.Ar, Ct.TA) and polar moment of inertia (pMOI), were significantly improved in DKO males but not females, compared to Sost-KO. However, cancellous bone properties in the distal femur and lumbar spine, including bone volume fraction (BV/TV), trabecular thickness (Tb.Th), and trabecular number (Tb.N), were significantly improved in DKO females but not males, compared to Sost-KO. Femur length at 20 weeks of age was not different among groups, suggesting that linear growth was not affected by either mutation singly or in combination (Fig.S2E). In summary, the μCT results suggest that Sostdc1 deletion significantly increases cortical properties in male mice and cancellous properties in female mice, but only on a Sost-deficient background (and not on a $Sost^{+/+}$ background).

Sost;Sostdc1-DKO male mice have improved biomechanical properties and increased periosteal bone formation compared to Sost KO mice.

We next examined the potential functional consequences of disabling Sostdc1 and Sost on bone mechanical properties, using 3-point bending tests on fresh-frozen femora from Sostdc1 and Sost mutants. As expected, femora from Sost-KO exhibited significant increases in the whole-bone mechanical properties ultimate force, stiffness, and energy absorption, compared to WT controls. However, femora from Sostdc1-KO were not different from WT. Consistent with μCT-derived cortical bone properties reported above, male but not female DKO mice yielded significant improvements in several properties, including ultimate force and stiffness, but not energy absorption, beyond those measured for Sost-KO samples (Fig 3A & B).

Analysis of histomorphometrically derived bone formation parameters at the femoral midshaft in both male and female DKO mice revealed significantly increased periosteal bone formation rates, compared Sost KO groups (Figs. 3C, 3D, S3A). The increase in periosteal BFR/BS among DKO mice was driven mainly by increases in MAR (Fig. S3A). Endosteal bone formation parameters were not affected by Sostdc1 deletion, with the exception of MS/BS and BFR/BS in male $Sost^{+/+}$ mice. No changes in osteoclast number or surface

in the distal femur primary spongiosa were detected between male Sdc and WT controls (Fig. S6). In summary, diaphyseal mechanical properties and periosteal bone formation rates were significantly improved by Sostdc1 deletion in male mice, but only on a Sost-deficient background (and not on a $Sost^{+/+}$ background).

Sostdc1 neutralizing antibody (Sdc-mAb) treatment alone has no effect on bone properties, but Sdc-mAb neutralization in the presence of sclerostin neutralizing antibody (Scl-mAb) improves cortical properties, compared to Scl-mAb alone

To translate the genetic mouse model findings and assess the therapeutic potential of dual inhibition of sclerostin and Sostdc1, we tested the efficacy of combining sclerostin monoclonal antibody (Scl-mAb) and Sostdc1 monoclonal antibody (Sdc-mAb) as a potential osteoanabolic treatment in WT mice, and compared the effects to each antibody alone (and to vehicle control; see Fig. 4A). Vehicle control mice were injected with an equal volume of saline buffer used to reconstitute antibody. Femur length and body mass were unaffected by the treatments (Fig. 4B & C). Compared to vehicle control, Sdc-mAb alone had no effect on skeletal properties, whether measured by DXA (Fig. 4D), μCT (Fig. 4E-4G & Fig. S4), mechanical testing (Fig. 5A & B), or histomorphometry (Fig. 5C & D). As expected, and consistent with previous experiments, Scl-mAb alone significantly improved skeletal properties in each of the endpoints measured. Whereas Sdc-mAb alone had no measurable effects, Sdc-mAb administered alongside Scl-mAb improved numerous skeletal endpoints significantly. Sdc-mAb/Scl-mAb treatment increased whole body BMD by 25% ($p<0.05$) beyond that generated by Scl-mAb alone (Fig. 4D). Partitioning the bone envelopes using μCT revealed that cancellous bone was unaffected by Sdc-mAb/Scl-mAb combination therapy, whereas cortical bone was significantly improved. Cortical thickness (Ct.Th), bone area (Ct.B.Ar), and polar moment (pMOI) in Sdc/Scl antibody treated mice were increased significantly, by 6-30%, beyond Scl-mAb treatment alone. None of the femoral or vertebral cancellous bone measurements showed any significant effect of combined therapy (Fig. 4E). Measurements of whole bone bending properties revealed a significant increase in the combined therapy group for stiffness, but not for peak force or energy (Fig. 5A & B). Surprisingly, midshaft femur bone formation rates were not different between Scl-mAb alone and the combined treatment group (Fig. 5C & 5D), despite a significant increase in many of the μCT-derived cortical properties.

DISCUSSION

Our primary goal in conducting these experiments was to determine whether the combination of Sostdc1 and Sost/sclerostin co-deletion or co-inhibition could improve cortical bone properties beyond additive effects of individual antagonist targeting. The scientific precedent for the investigation was based on previous work showing that co-inhibition of sclerostin and Dkk1—another Wnt antagonist—had potentiating effects in the trabecular compartment. Here, the focus was on exploring a combination that might have the same potentiating effects, but in the cortical compartment. Significant potentiation of the Sostdc1 deletion effects via Sost deletion were achieved only in male mice, as revealed by an increase in most cortical parameters (mid-femur μCT properties, mid-femur bending tests, mid-femur bone formation rates) beyond Sost deletion alone, whereas Sostdc1

deletion alone had very few detectable effects. Although the cortical bone compartment in female mice was not additionally affected by Sost;Sostdc1 co-deletion, it was responsive to co-inhibition of Sostdc1 and sclerostin, as revealed by a significant improvement in cortical properties among dual-antibody treated mice, compared to Scl-mAb alone.

In a previous paper, we reported a significant increase in cortical bone properties and a significant decrease in cancellous bone properties, among ~6 month-old male Sostdc1$^{-/-}$ mice.[12] In the present communication, we were unable to reproduce these phenotypes in male or female Sostdc1$^{-/-}$ mice, though the mice studied here were younger. Despite the lack of cortical phenotype in single Sostdc1 mutants, the propensity of Sostdc1 deletion to increase cortical bone mass was manifest when those alleles were moved onto a Sost$^{-/-}$ background. Similarly, Sdc-mAb treatment alone was not associated with a cortical bone phenotype, but Sdc-mAb in the presence of Scl-mAb was able to bring forth the cortical phenotype reported earlier. This scenario is similar to one we previously reported[13] for the Scl-mAb/Dkk1-mAb effect on cancellous bone: whereas Dkk1-mAb treatment alone had no consistent effect on cancellous bone, Dkk1-mAb treatment in the presence of Scl-mAb (or injected into Sost$^{-/-}$ mice) was able to bring forth a strong cancellous phenotype. We have repeated that experiment several times in different contexts (varying the drug dose, ratio of components, and age) and have consistently found a strong potentiation in the cancellous compartment, but the cortical compartment was rarely affected by dual treatment (including both endocortical and periosteal parameters). Others have confirmed the positive cancellous and neutral cortical effects of this combination[14] One of the reasons we looked at Sostdc1 in combination with sclerostin inhibition was to determine whether we could improve cortical bone *per se.*

Identification of potentiating partnerships for targeting has several advantages to monotherapy, including the ability to lower total drug dose (reduced cost), less risk for adverse events from any given targeting strategy, and propensity for a stronger response. An added benefit is the ability to achieve more compartmentalized control of the anabolic response, which could be advantageous in situations where cancellous but not cortical enhancement is desired, or vice versa.

While Sostdc1 is most closely to Sost among all the DAN family members,[26] the two protein products share only ~40% amino acid homology.[27] Both can bind Lrp5/6 and inhibit Wnt signaling,[28] but Sostdc1 is a much stronger inhibitor of bone morphogenetic proteins (Bmps) than sclerostin.[10] Further, sclerostin exhibits greater affinity for Lrp5/6,[17, 29] whereas Sostdc1 exhibits greater affinity for Lrp4[30]—a facilitator protein that supports Sost and Sostdc1 interaction with Lrp5/6.[31] Sostdc1$^{-/-}$ mice have a dental phenotype that is characterized by supernumerary molars,[32] an effect absent in Sost$^{-/-}$ mice. Recent evidence suggests that Sostdc1 protein normally exists as a dimer, whereas sclerostin exists as a monomer, which contributes to the predilection for Bmps by Sostdc1 but not sclerostin.[10]

A great deal more is known about Sost/sclerostin than for Sostdc1, likely a result of the intensive effort to develop sclerostin neutralization as a clinical tool to prevent fractures. Sostdc1 is enriched in the periosteal layer of long bones, which might explain the enhanced

effect we observed on periosteal bone formation rates in the double knockouts. As the periosteum is a rich source of mesenchymal stem progenitor cells that support fracture healing, it might also explain why Sostdc1 mutants are able to heal long bone fractures more quickly.[12]

There are several limitations to our study. First, we used mice with global deletion of both Sost and Sostdc1. While this approach is useful for modeling the pharmacologic effects of protein loss/inhibition body-wide (as most osteoporosis drugs are delivered systemically), it does not provide any information on the cell type of action for the effects observed. The same drawback is true of the antibody-based studies we conducted. Floxed mice have been developed and published for Sost[33] but currently we are unaware of any Sostdc1-flox mouse models. Second, while the combination of Sost and Sostdc1 deletion improved cortical bone properties in male mice, and the Scl-mAb/Sdc-mAb improved cortical bone in female mice, the effect size of the improvement was not of the same magnitude we observed in the cancellous compartment for Sost/Dkk1 combinations. Thus, it is unclear whether the additional benefit to the cortex that might be gained from targeting both sclerostin and Sostdc1 would justify their clinical development. It is curious that female mice responded robustly to combination antibody treatment, but not to compound genetic deletion. This might reflect an effect of chronic vs. acute inhibition, but it would be difficult to determine given our experimental design. Further, the sex-specific effects observed for the genetic models (we tested antibody only in one sex due to reagent limitations) might restrict applicability of Sost/Sostdc1 targeting as a therapy. Interestingly, there are clinical data suggesting that genetic polymorphisms in SOSTDC1 have an effect on attainment and maintenance of peak bone mass in women but not men.[34] Another factor limiting the impact of our studies is the potential for unaccounted negative feedback loops among other inhibitors. As Wnt inhibitors exhibit complex compensatory expression profiles, there might be other unaccounted factors that change expression during sclerostin/Sostdc1 inhibition that restrain an otherwise more anabolic effect of the combination. We have observed the effects of this compensatory milieu for other Wnt antagonists but it might also cross over into other pathways like Shh or Bmp due to Sostdc1's more widespread effects.[35] Additionally, we did not include a low-dose combination group for the antibody studies. It is possible that sclerostin inhibition has such strong effects on all bone envelopes that much lower doses of Scl-mAb are required to observe a fuller effect of inhibition of synergistic partners. Lastly, it is unclear whether there were unwanted side effects induced by dual antibody treatment. Sostdc1 is also known to be highly expressed in the kidney; global deletion of Sostdc1 confers renal protection in a mouse model of Alport syndrome,[36] and Sdc-mAb protects against fibrosis in a renal injury model.[18, 21] Upon sacrifice and necropsy, the kidneys of Sostdc1$^{-/-}$ and Sdc-mAb-treated mice were unremarkable and normal in appearance, but we did not conduct any phenotyping on this organ.

In summary, the experiments suggest that disabling both Sost/sclerostin and Sostdc1 provides skeletal benefits beyond Sost/sclerostin targeting alone, particularly in the cortical bone, even though we observed no effect of disabling Sostdc1 alone. The effects were sex-specific, as surprisingly, chronic deletion of both Sost and Sostdc1 improved cancellous rather than cortical bone in female mice. Our findings indicate that Wnt-based synergistic osteoanabolism is possible in the cortex, particularly in conjunction with sclerostin

neutralization, but additional targets will need to be identified to produce an effect size that is worthy of clinical use.

Supplementary Material

Refer to Web version on PubMed Central for supplementary material.

Acknowledgments

Financial support was provided by the NIH (AR053237 to AGR; AG069489 to RBC; DK075730 to GGL), the US Department of Veterans Affairs (BX001478 and BX003783 to AGR) and the US Department of Energy (DE-AC52-07NA27344 to GGL). Sclerostin and Sostdc1/Wise antibodies were provided by Amgen Inc. and UCB (Brussels, Belgium). The content is solely the responsibility of the authors and does not necessarily represent the official views of the NIH. The funders had no role in study design, data collection and analysis, decision to publish, or preparation of the manuscript.

References

1. Pallin DJ, Espinola JA, Camargo CA Jr., US population aging and demand for inpatient services. J Hosp Med 9, 193–196 (2014). [PubMed: 24464735]
2. Isojima T, Sims NA, Cortical bone development, maintenance and porosity: genetic alterations in humans and mice influencing chondrocytes, osteoclasts, osteoblasts and osteocytes. Cell Mol Life Sci 78, 5755–5773 (2021). [PubMed: 34196732]
3. Choi RB et al. , Notum Deletion From Late-Stage Skeletal Cells Increases Cortical Bone Formation and Potentiates Skeletal Effects of Sclerostin Inhibition. J Bone Miner Res 36, 2413–2425 (2021). [PubMed: 34223673]
4. Zheng HF et al. , WNT16 influences bone mineral density, cortical bone thickness, bone strength, and osteoporotic fracture risk. PLoS Genet 8, e1002745 (2012). [PubMed: 22792071]
5. Bennett CN et al. , Wnt10b increases postnatal bone formation by enhancing osteoblast differentiation. J Bone Miner Res 22, 1924–1932 (2007). [PubMed: 17708715]
6. Kiper POS et al. , Cortical-Bone Fragility--Insights from sFRP4 Deficiency in Pyle's Disease. N Engl J Med 374, 2553–2562 (2016). [PubMed: 27355534]
7. Yanagita M et al. , USAG-1: a bone morphogenetic protein antagonist abundantly expressed in the kidney. Biochem Biophys Res Commun 316, 490–500 (2004). [PubMed: 15020244]
8. Kim J et al. , Shh Plays an Inhibitory Role in Cusp Patterning by Regulation of Sostdc1. J Dent Res 98, 98–106 (2019). [PubMed: 30325689]
9. Faraahi Z, Baud'huin M, Croucher PI, Eaton C, Lawson MA, Sostdc1: A soluble BMP and Wnt antagonist that is induced by the interaction between myeloma cells and osteoblast lineage cells. Bone 122, 82–92 (2019). [PubMed: 30776499]
10. Gipson GR, Kattamuri C, Czepnik M, Thompson TB, Characterization of the different oligomeric states of the DAN family antagonists SOSTDC1 and SOST. Biochem J 477, 3167–3182 (2020). [PubMed: 32779697]
11. Togo Y et al. , Antagonistic Functions of USAG-1 and RUNX2 during Tooth Development. PLoS One 11, e0161067 (2016). [PubMed: 27518316]
12. Collette NM et al. , Sostdc1 deficiency accelerates fracture healing by promoting the expansion of periosteal mesenchymal stem cells. Bone 88, 20–30 (2016). [PubMed: 27102547]
13. Witcher PC et al. , Sclerostin neutralization unleashes the osteoanabolic effects of Dkk1 inhibition. JCI Insight 3 (2018).
14. Florio M et al. , A bispecific antibody targeting sclerostin and DKK-1 promotes bone mass accrual and fracture repair. Nat Commun 7, 11505 (2016). [PubMed: 27230681]
15. Choi RB et al. , Improving Bone Health by Optimizing the Anabolic Action of Wnt Inhibitor Multitargeting. JBMR Plus 5, e10462 (2021). [PubMed: 33977198]

16. Choi RB et al. , Targeting Sclerostin and Dkk1 at Optimized Proportions of Low-Dose Antibody Achieves Similar Skeletal Benefits to Higher-Dose Sclerostin Targeting in the Mature Adult and Aged Skeleton. Aging Dis 13, 1891–1900 (2022). [PubMed: 36465166]
17. Collette NM, Genetos DC, Murugesh D, Harland RM, Loots GG, Genetic evidence that SOST inhibits WNT signaling in the limb. Dev Biol 342, 169–179 (2010). [PubMed: 20359476]
18. Yanagita M et al. , Uterine sensitization-associated gene-1 (USAG-1), a novel BMP antagonist expressed in the kidney, accelerates tubular injury. J Clin Invest 116, 70–79 (2006). [PubMed: 16341262]
19. Worlein JM, Baker K, Bloomsmith M, Coleman K, Koban TL, The Eighth Edition of the Guide for the Care and Use of Laboratory Animals (2011); Implications for Behavioral Management. Am J Primatol 73, 98–98 (2011).
20. Li X et al. , Inhibition of sclerostin by monoclonal antibody increases bone formation, bone mass, and bone strength in aged male rats. J Bone Miner Res 25, 2647–2656 (2010). [PubMed: 20641040]
21. Qian X et al. , Inhibition of WISE preserves renal allograft function. J Am Soc Nephrol 24, 66–76 (2013). [PubMed: 23184054]
22. Bouxsein ML et al. , Guidelines for assessment of bone microstructure in rodents using micro-computed tomography. J Bone Miner Res 25, 1468–1486 (2010). [PubMed: 20533309]
23. Dempster DW et al. , Standardized Nomenclature, Symbols, and Units for Bone Histomorphometry: A 2012 Update of the Report of the ASBMR Histomorphometry Nomenclature Committee. Journal of Bone and Mineral Research 28, 1–16 (2013). [PubMed: 23255454]
24. Kang KS et al. , Induction of Lrp5 HBM-causing mutations in Cathepsin-K expressing cells alters bone metabolism. Bone 120, 166–175 (2019). [PubMed: 30409757]
25. Turner CH, Burr DB, Basic biomechanical measurements of bone: a tutorial. Bone 14, 595–608 (1993). [PubMed: 8274302]
26. Opazo JC, Hoffmann FG, Zavala K, Edwards SV, Evolution of the DAN gene family in vertebrates. Dev Biol 482, 34–43 (2022). [PubMed: 34902310]
27. Kusu N et al. , Sclerostin is a novel secreted osteoclast-derived bone morphogenetic protein antagonist with unique ligand specificity. J Biol Chem 278, 24113–24117 (2003). [PubMed: 12702725]
28. Ellies DL et al. , Bone density ligand, Sclerostin, directly interacts with LRP5 but not LRP5G171V to modulate Wnt activity. J Bone Miner Res 21, 1738–1749 (2006). [PubMed: 17002572]
29. van Dinther M et al. , Anti-Sclerostin antibody inhibits internalization of Sclerostin and Sclerostin-mediated antagonism of Wnt/LRP6 signaling. PLoS One 8, e62295 (2013). [PubMed: 23638027]
30. Ohazama A et al. , Lrp4 modulates extracellular integration of cell signaling pathways in development. PLoS One 3, e4092 (2008). [PubMed: 19116665]
31. Bullock WA et al. , Lrp4 Mediates Bone Homeostasis and Mechanotransduction through Interaction with Sclerostin In Vivo. iScience 20, 205–215 (2019). [PubMed: 31585407]
32. Kassai Y et al. , Regulation of mammalian tooth cusp patterning by ectodin. Science 309, 2067–2070 (2005). [PubMed: 16179481]
33. Economides AN et al. , Conditionals by inversion provide a universal method for the generation of conditional alleles. Proc Natl Acad Sci U S A 110, E3179–3188 (2013). [PubMed: 23918385]
34. He JW, Yue H, Hu WW, Hu YQ, Zhang ZL, Contribution of the sclerostin domain-containing protein 1 (SOSTDC1) gene to normal variation of peak bone mineral density in Chinese women and men. J Bone Miner Metab 29, 571–581 (2011). [PubMed: 21221677]
35. Ahn Y, Sanderson BW, Klein OD, Krumlauf R, Inhibition of Wnt signaling by Wise (Sostdc1) and negative feedback from Shh controls tooth number and patterning. Development 137, 3221–3231 (2010). [PubMed: 20724449]
36. Tanaka M et al. , Loss of the BMP antagonist USAG-1 ameliorates disease in a mouse model of the progressive hereditary kidney disease Alport syndrome. J Clin Invest 120, 768–777 (2010). [PubMed: 20197625]

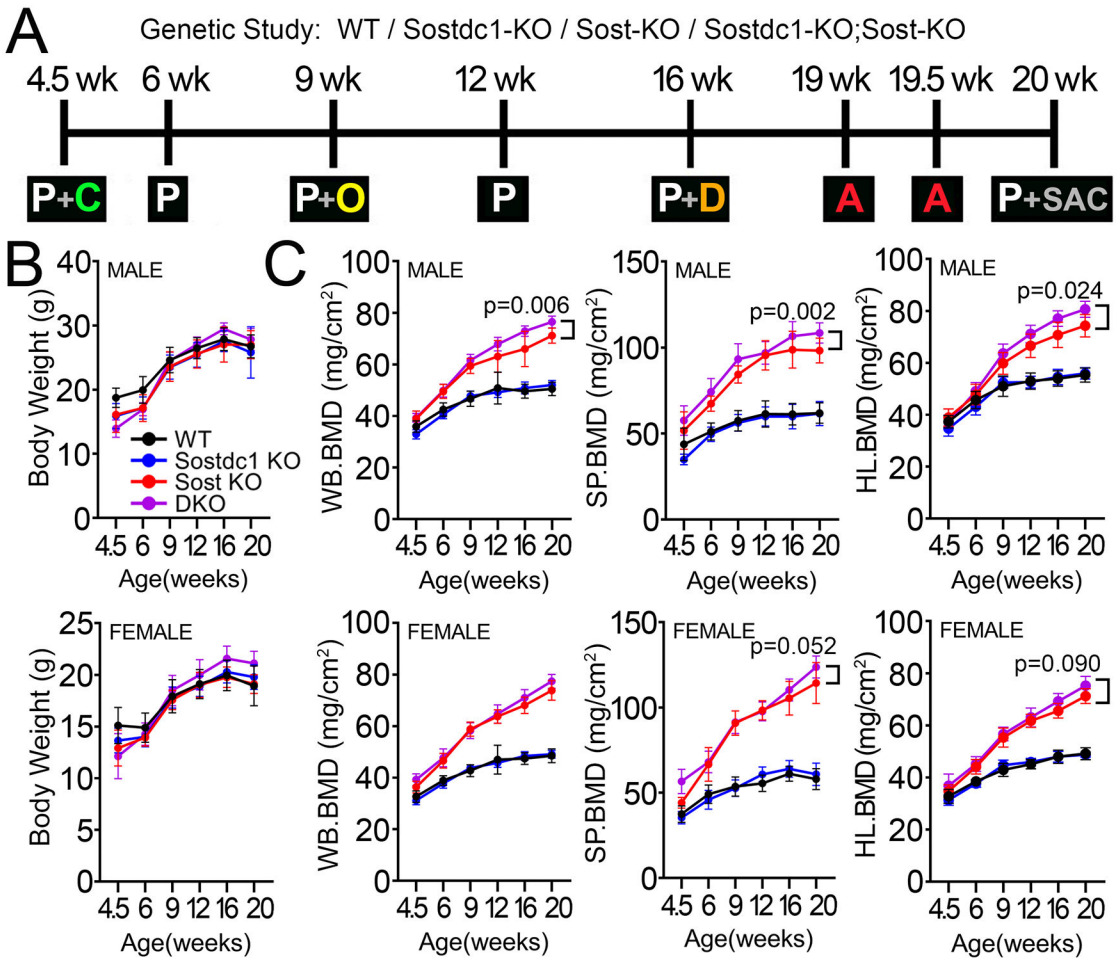

Figure 1. Genetic deletion of Sostdc1 improves bone mineral density and bone mineral content in the absence of sclerostin, but only for male mice.

(A) Experimental schematic of genetic study involving wild-type (WT), Sostdc1 knockout (Sostdc1-KO), Sost knockout (Sost-KO) and Sostdc1/Sost double knockout (DKO) mice. Mouse age spans across the top of the diagram with key ages indicated for various procedures. P=PIXIMUS (DXA); C=calcein injection; O=oxytetracycline injection; D=demeclocycline injection; A=alizarin injection; SAC = sacrifice and necropsy.

(B) Serial measurements of body mass in all four genotypes (males in top panel, females in bottom panel)

(C) Serial measurements of bone mineral density (BMD) calculated at various regions of interest, including whole body (WB), lumbar spine (SP), and hindlimb (HL), from dual-energy X-ray absorptiometry (DXA) scans. For sample sizes, Male: WT: n=13, Sostdc1-KO: n=10, Sost-KO: n=12, Sost;Sostdc1 DKO: n=11. Female: WT: n=10, Sostdc1-KO: n=11, Sost KO: n=11, Sost;Sostdc1 DKO: n=10. Data were analyzed using repeated-measures one-way ANOVA followed by Tukey post-hoc tests.

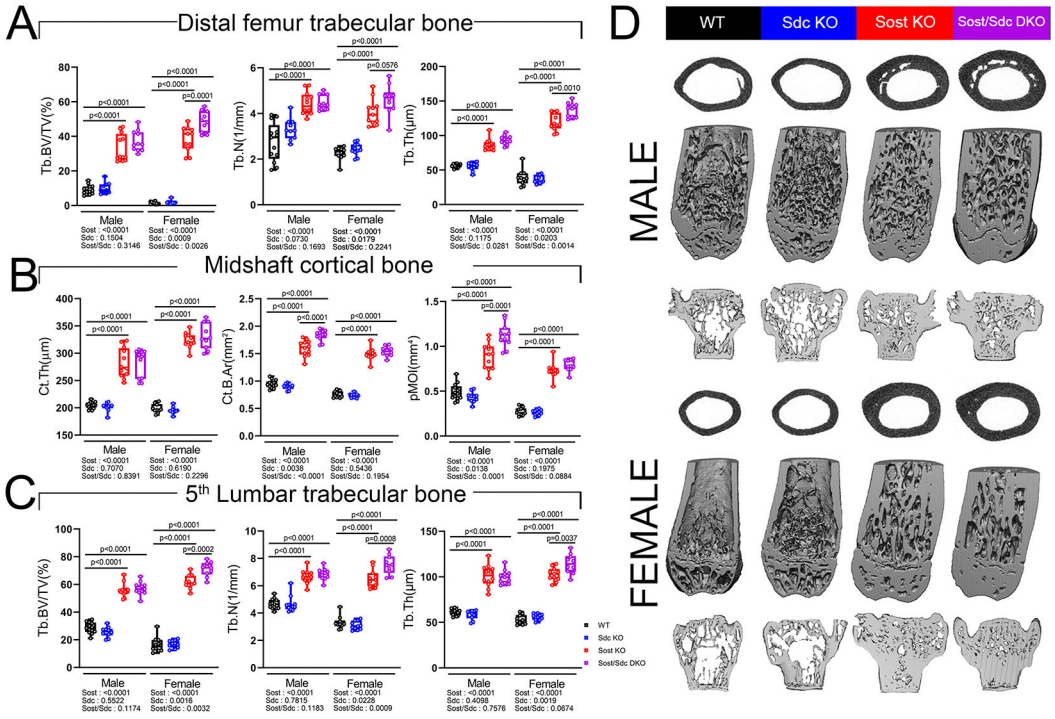

Figure 2. Genetic co-deletion of Sost and Sostdc1 improves long bone cortical bone properties in male mice and cancellous properties in female mice.

(A) μCT-derived trabecular bone volume fraction (Tb.BV/TV), trabecular number (Tb.N) and trabecular thickness (Tb.Th) at the distal femoral metaphysis of 20-wk-old wild-type (WT), Sostdc1-knockout (Sdc-KO), Sost knockout (Sost-KO), and Sostdc1;Sost double knockout (DKO) mice. **(B)** μCT-derived cortical bone thickness (Ct.Th), cortical bone area (Ct.B.Ar), and polar moment of inertia (pMOI) at the femoral midshaft of 20-wk-old WT, Sostdc1-KO, Sost-KO, and DKO mice. **(C)** μCT-derived trabecular bone properties Tb.BV/TV, Tb.N, and Tb.Th at the 5th lumbar vertebra collected from 20-wk-old WT, Sostdc1-KO, Sost-KO, and DKO mice. **(D)** Representative midshaft femur (upper row), distal femur (middle row) and lumbar vertebra (lower row) μCT reconstructions from 20-wk-old male and female mice. For sample sizes, Male: WT: n=13, Sostdc1-KO: n=10, Sost-KO: n=12, Sost;Sostdc1 DKO: n=11. Female: WT: n=10, Sostdc1-KO: n=11, Sost-KO: n=11, Sost;Sostdc1 DKO: n=10. All data were analyzed by two-way ANOVA followed by Tukey post hoc tests. The significance of each main effect (i.e., gene) and interaction term (Sostdc1 × Sost) in the two-way model appear beneath each sex-specific section of the panels.

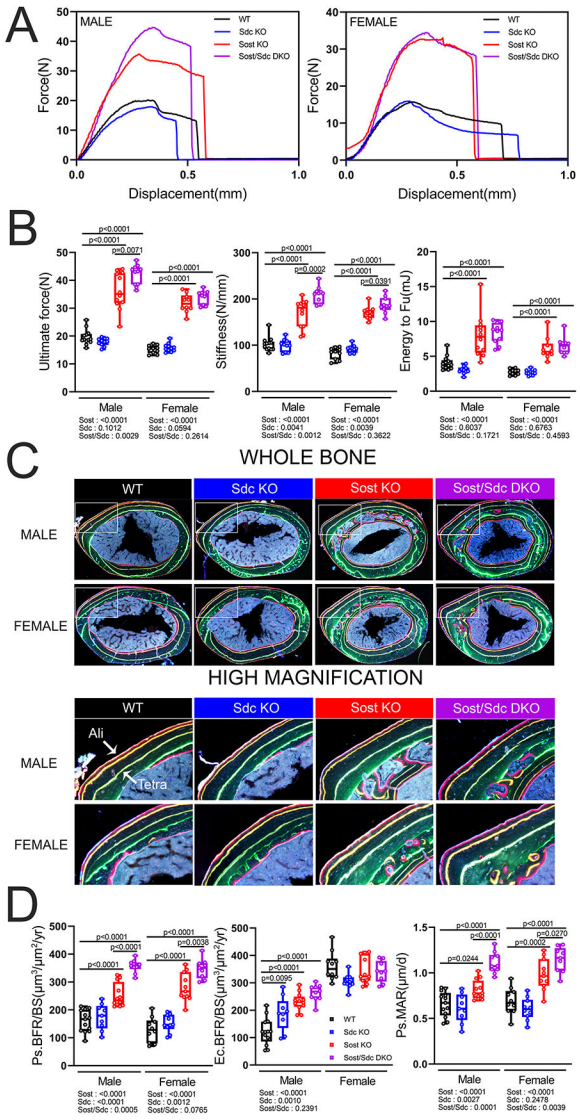

Figure 3. Genetic co-deletion of Sost and Sostdc1 improves mechanical properties in male mice and increases periosteal bone formation in both sexes.

(A) Representative force- displacement curves from three-point monotonic bending tests to failure conducted on whole femurs from 20-wk-old male and female wild-type (WT), Sostdc1 knockout (Sostdc1-KO), Sost knockout (Sost-KO) and Sostdc1/Sost double knockout (DKO) mice. **(B)** Quantification of ultimate force (peak height of the curve in panel A), stiffness (slope of the linear portion of the curve in panel A) and energy absorbed (area under the curve in A) from 20-wk-old male and female mice. **(C)** Representative fluorochrome-labeled midshaft femur histologic cross-sections from 20-wk-old male and female mice. The ROI box in the whole bone panels is magnified in the right panels to visualize bone formation between the yellow tetracycline label (labeled “Tetra”) and the middle of double red alizarin complexone labels (labeled “Ali”), respectively. See Figure 1A for labeling schedule. **(D)** Quantification of anabolic action on the periosteal (Ps) and endocortical (Ec) surfaces, calculated as the bone formation rate per unit bone surface (BFR/BS)(left and middle panel) and the mineral apposition rate (MAR)(right panel). For

sample sizes, (Panel B) Male: WT: n=13, Sostdc1-KO: n=10, Sost-KO: n=12, Sost;Sostdc1 DKO: n=11. Female: WT: n=10, Sostdc1-KO: n=11, Sost-KO: n=11, Sost;Sostdc1 DKO: n=10; (Panel D) Male: WT n=13, Sostdc1-KO: n=9, Sost-KO: n=12, Sost;Sostdc1 DKO: n=10. Female: WT: n=10, Sostdc1-KO: n=10, Sost-KO: n=11, Sost;Sostdc1 DKO: n=9. All data were analyzed by Two-way ANOVA followed by Tukey post hoc tests. The significance of each main effect (i.e., gene) and interaction term (Sostdc1 × Sost) in the two-way model appear beneath each sex-specific section of the panels.

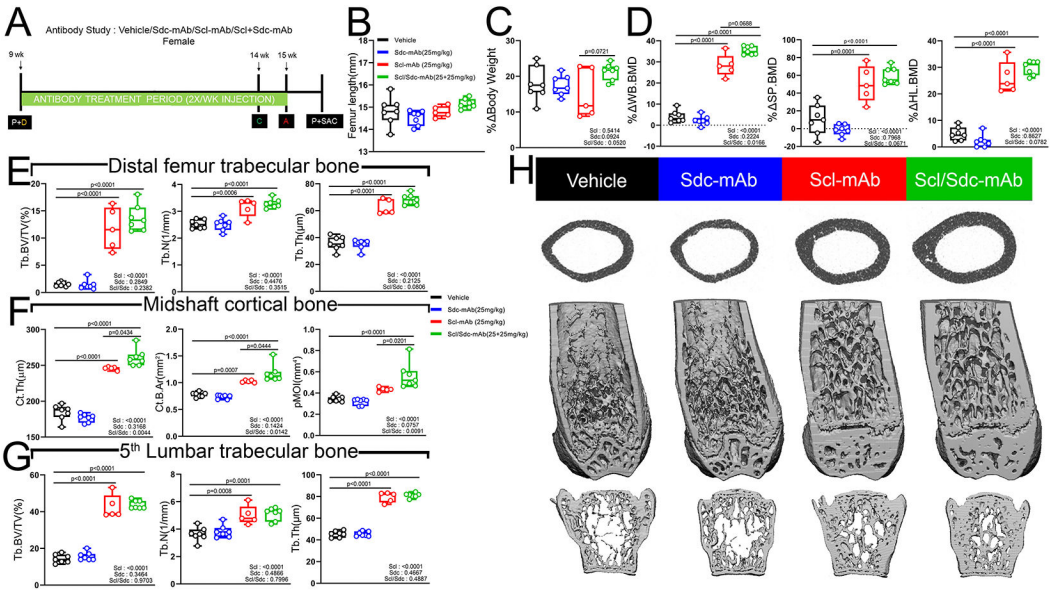

Figure 4. Sostdc1 antibody has no effect on bone properties when administered alone, but coadministration with Scl-mAb confers cortical bone efficacy.

(A) Experimental plan for antibody study, conducted in 9-wk-old female WT C57BL/6J mice. P=PIXIMUS (DXA); D=demeclocycline injection; C=calcein injection; A=alizarin injection; SAC = sacrifice and necropsy.

(B) Femur length at sacrifice (16 wks of age) among mice receiving 25 mg/kg of sclerostin antibody (Scl-mAb), 25 mg/kg of Sostdc1 antibody (Sdc-mAb), or a 1:1 mixture of Scl-mAb and Sdc-mAb at 25 mg/kg each.

(C) Percent change in body mass among all treatment groups calculated using beginning (9 wks) and final (16 wks) measurements. **(D)** DXA-derived changes (%Δ) in bone mineral density (BMD), calculated using beginning (9 wks) and final (16 wks) measurements at 3 regions of interest: whole body (WB), lumbar spine (SP) and entire right hindlimb distal to the acetabulum (HL). **(E)** μCT-derived trabecular bone volume fraction (Tb.BV/TV), thickness (Tb.Th) and number (Tb.N) in the distal femoral metaphysis among all treatment groups, at 16 wks of age. **(F)** μCT-derived cortical bone thickness (Ct.Th), cortical bone area (Ct.B.Ar), and polar moment of inertia (pMOI) at the femoral midshaft among the four treatment groups, at 16 wks of age.

(G) μCT-derived trabecular bone volume fraction (Tb.BV/TV), trabecular thickness (Tb.Th) and trabecular number (Tb.N) in the 5^{th} lumbar vertebrae among all treatment groups, at 16 wks of age. **(H)** Representative μCT reconstructions of the femoral midshaft, distal third of the femur (ventral view with the anterior half digitally removed), and lumbar vertebra (lower row) from each treatment group, revealing the effects of combination therapy in cortical but not cancellous bone. For sample sizes, Vehicle : n=7, Sdc-mAb: n=7, Scl-mAb: n=5, Scl/Sdc-mAb: n=7. All data were analyzed by two-way ANOVA followed by Tukey post hoc tests. The significance of each main effect (i.e., each antibody) and interaction term (Scl-mAb × Sdc-mAb) in the two-way model appear in the bottom right corner of each panel.

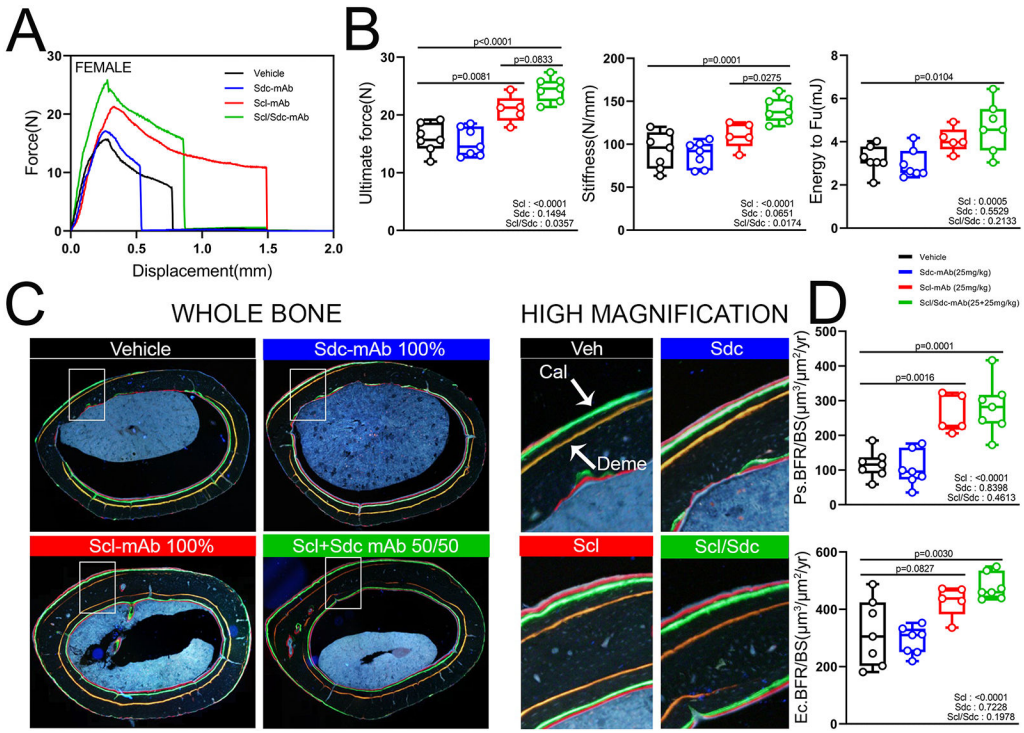

Figure 5. Select cortical bone mechanical properties but not formation indices are improved by combination Sost/Sostdc1 antibody therapy.

(A) Representative force- displacement curves from three-point monotonic bending tests to failure conducted on whole femurs from 16-wk old female WT mice treated with vehicle, Sostdc1 antibody (Sdc-mAb) alone, sclerostin antibody (Scl-mAb) alone, or a 1:1 mixture of Scl-mAb and Sdc-mAb **(B)** Quantification of ultimate force (peak height of the curve in panel A), stiffness (slope of the linear portion of the curve in panel A) and energy absorbed (area under the curve in A). **(C)** Representative fluorochrome-labeled midshaft femur histologic cross-sections from mice treated as described for panel A. The ROI box in the whole bone panels is magnified in the right panels to visualize bone formation between the orange demeclocycline label and the green calcein labels, respectively. See Figure 4A for labeling schedule. **(D)** Quantification of anabolic action on the periosteal (Ps) and endocortical (Ec) surfaces, calculated as the bone formation rate per unit bone surface (BFR/BS). For sample sizes, Vehicle: n=7, Sdc-mAb: n=7, Scl-mAb: n=5, Scl/Sdc-mAb: n=7. All data were analyzed by two-way ANOVA followed by Tukey post hoc tests. The significance of each main effect (i.e., each antibody) and interaction term (Scl-mAb × Sdc-mAb) in the two-way model appear in the bottom right corner of each panel.